

Modeling Hybrid AC/DC Power Systems with the Complex Frequency Concept

Ignacio Ponce, *Member, IEEE*, and Federico Milano, *Fellow, IEEE*

Abstract—The concept of complex frequency has been recently introduced on the IEEE Transactions on Power Systems to study bus voltage variations in magnitude and frequency and their link with complex power injections of a power system. In this paper, the complex frequency is applied to time-varying series connections, namely, RLC dynamic branches, regulating transformers and AC/DC converters. The proposed modeling approach allows deriving an explicit expression for the complex frequency of the voltage of a certain bus as a linear combination of three elements: net current injected by the devices connected to the bus, adjacent voltages, and time-varying series branches. The proposed formulation unifies the link between voltage and frequency dynamics in AC, DC, as well as hybrid AC/DC power systems. A variety of static and dynamic examples are presented to show the potential of the proposed formulation. Relevant applications of the proposed modeling approach are outlined.

Index Terms—Hybrid AC/DC power systems, power system modeling, power system dynamic performance, complex frequency (CF).

I. INTRODUCTION

A. Motivation

The dynamic behavior of power systems is experiencing unprecedented changes due to the increasing penetration of converter-interfaced devices. Several recent works have discussed the challenges this transition is posing to the modeling, control, and stability analysis of power systems [1]–[5]. Among these challenges, the most relevant for this paper is the need to revisit some fundamental aspects of the modeling of power systems. In particular, recent works have highlighted the relevance of a more accurate definition and interpretation of the frequency of power systems [6]–[8]. A novel quantity, the complex frequency (CF), has been introduced recently in [9] precisely to provide a more consistent foundation for the analysis of frequency variations in AC power systems. The most relevant feature of the CF is the ability to link the variations of the complex power and the variations of the voltage in magnitude and frequency in a common framework. This paper focuses on elaborating on the use of this concept and further exploiting its potential.

B. Literature Review

The complex frequency has been used recently in promising applications in power systems modeling. For example, it is shown in [10] that the differential-algebraic equations that

describe the grid dynamics can be rewritten solely in terms of the CF and state variables, removing completely the dependence on voltage magnitudes and angles. CF has also already found relevant applications in control [11], [12], converter synchronization [13], [14], and state estimation [15], [16]. A relevant example is provided in [17], where the concept is used to describe and classify different control schemes and synchronization mechanisms of power converters. Although originally applied to voltages and currents, the CF concept can be also applied to any time-varying complex quantity. In this paper, we define the CF of time-varying admittances, which allows describing any series element that can be modeled through an equivalent circuit.

The relationship between the CF at a bus and the complex powers was originally presented in [9] through an implicit equation, where two types of contributions are distinguished. On one side of the equation, the terms correspond to voltage variations and complex powers coming from neighbor buses connected through a constant admittance, and they are said to be the network contribution. On the other side, the CF of the bus and the variations of the complex power of every other element, referred to as the device's contribution. Under this formulation, active series devices whose model is different from a constant admittance block are treated similarly to shunt devices instead of branches. Thus, the effect of neighbor buses connected through regulating transformers, AC/DC converters and other special series connections cannot be directly evaluated. The extension of the use of the CF to admittances allows a more general and consistent formulation where the effect of neighbor buses is represented in the same way whether they are connected through an active series device or not. This approach allows us deriving an explicit equation for the CF of the voltage of a bus with separate terms for the effect of local shunt devices, the network, and dynamic connections.

The aforementioned approach is particularly useful to study the dynamic behavior of AC/DC converters. In particular, we analyze the dynamic link between AC- and DC-side dynamics, which depend on the controllers configured on the converter. This study is relevant as the dynamic interaction of the converter's AC and DC circuits has been shown to have a significant impact on the dynamic performance of the system. For instance, authors in [18] show that for wind farms connected through an MMC-HVDC interconnection, depending on the control mode, there might be a threat to the stability of the DC side and undesirable oscillations on the AC side. The formulation proposed in this work treats the converter as any other series branch, thus giving the ability to relate the CF of the voltage at the AC and DC sides using a single framework.

I. Ponce and F. Milano are with School of Electrical and Electronic Engineering, University College Dublin, Belfield Campus, D04V1W8, Ireland. e-mails: ignacio.poncearancia@ucdconnect.ie, federico.milano@ucd.ie

This work is supported by the Sustainable Energy Authority of Ireland (SEAI) by funding I. Ponce and F. Milano under project FRESLIPS, Grant No. RDD/00681.

C. Contributions

The two main contributions of the paper are as follows:

- A systematic approach to model, based on the concept of CF, the dynamic behavior of different time-varying branches.
- An explicit expression of the CF of the voltage of every bus of the system as a linear function of the net current injected by shunt devices at the bus, the effect of time-varying branches connected to the bus, and the CF of the voltage of neighbor buses.

The proposed framework is *general*, as it unifies the modeling of AC, DC or hybrid AC/DC power systems. The approach is also *systematic* as long as the series element can be modeled through an admittance block. Finally, the formulation of the bus CFs is *exact* and does not require any assumption on the model of the devices connected to the branch.

D. Paper Organization

The remainder of this paper is organized as follows. Section II provides a general definition and the notation utilized in the remainder of the paper. Section III presents the proposed explicit equation for the complex frequency. Specific expressions for the admittance model and the CF of different types of time-varying branches are presented in Section IV. The implementation of the proposed formulation in three study cases is described in Section V, and some remarks on its potential applications are provided in Section V-D. Finally, Section VI presents the conclusions and proposes future work.

II. BACKGROUND

The complex frequency is, in turn, a derivative operator of a complex number. In fact, any complex quantity, say \bar{u} , with non-null magnitude, i.e., $|\bar{u}| = u \neq 0$, can be written as:

$$\bar{u} = \exp(\kappa + j\theta), \quad (1)$$

where $\kappa = \ln(u)$. If κ and θ are smooth functions of time, the time derivative of \bar{u} gives:

$$\dot{\bar{u}} = \frac{d\bar{u}}{dt} = (\dot{\kappa} + j\dot{\theta}) \exp(\kappa + j\theta) = \left(\frac{\dot{u}}{u} + j\dot{\theta} \right) \bar{u}. \quad (2)$$

In the remainder of this paper, the quantity $(\frac{\dot{u}}{u} + j\dot{\theta})$ is called *complex frequency*. We define and utilize the CF of several quantities, including voltages, currents and admittances. The following notation is used:

- $\bar{\eta}$ is the CF of voltage Park vectors,¹ namely $\dot{\bar{v}} = \bar{\eta} \bar{v}$. For economy of notation, we also define $\bar{\eta} = \rho + j\omega$, where $\rho = \dot{v}/v$ and $\omega = \dot{\theta}$.
- $\bar{\xi}$ is the CF of current Park vectors, namely $\dot{\bar{i}} = \bar{\xi} \bar{i}$.
- $\bar{\chi}$ is the CF of time-varying admittances, namely $\dot{\bar{Y}} = \bar{\chi} \bar{Y}$.

It can be shown that the CF is an invariant geometrical quantity, that is, its value is the same independently from the reference frame utilized to define the Park vector [19].

¹The interested reader can find a discussion on the definition of Park vectors, which, in turn, are sort of dynamic phasors in [8].

It may be useful to note that the CF is a derived physical quantity. It has thus nothing to do with the complex variable s of the Laplace transform that is widely utilized to study the frequency response of circuits and control systems. As a matter of fact, CF can be defined both in the time-domain and in the s -domain of the Laplace transform. In the remainder of this work, we consider only the time-domain.

III. PROPOSED FORMULATION

In this section, we derive an expression for the CF of the voltage of every bus as a linear combination of the CFs of neighbor voltages, the current injection at the bus, and the admittance connected to the bus.

Consider a network with n buses. We denote the set of the network buses as \mathbb{B} and the subset of buses containing every bus except one bus h as $\mathbb{B}_h = \mathbb{B} \setminus \{h\}$. The starting point is the equation of the current balance of a node $h \in \mathbb{B}$:

$$\bar{i}_h = \sum_{k \in \mathbb{B}_h} \bar{i}_{h \rightarrow k} = \sum_{k \in \mathbb{B}_h} (\bar{v}_h - \bar{v}_k) \bar{Y}_{hk}, \quad (3)$$

where \bar{i}_h is the net current injection at bus h from every device connected to h . It is important to remark that there is no assumption on the expression of \bar{Y}_{hk} . It can represent the admittance of any series element, dynamic or not, connected between nodes h and k .

Isolating \bar{v}_h from (3):

$$\bar{v}_h \sum_{k \in \mathbb{B}_h} \bar{Y}_{hk} = \sum_{k \in \mathbb{B}_h} \bar{v}_k \bar{Y}_{hk} + \bar{i}_h. \quad (4)$$

We denote $\bar{Y}_{hh} = -\sum_{k \in \mathbb{B}_h} \bar{Y}_{hk}$ similarly to how the diagonal elements of the admittance matrix of a power system are defined. Thus (4) can be equivalently written as:

$$-\bar{v}_h \bar{Y}_{hh} = \sum_{k \in \mathbb{B}_h} \bar{v}_k \bar{Y}_{hk} + \bar{i}_h. \quad (5)$$

Differentiating (5) and recalling the property of the CF to act as a linear derivative operator [9]:

$$-\bar{v}_h \bar{Y}_{hh} (\bar{\eta}_h + \bar{\chi}_{hh}) = \sum_{k \in \mathbb{B}_h} \bar{v}_k \bar{Y}_{hk} (\bar{\eta}_k + \bar{\chi}_{hk}) + \bar{i}_h \bar{\xi}_h, \quad (6)$$

where $\bar{\eta}_h$ is the CF of the voltage of bus h ; $\bar{\xi}_h$ is the CF of the net current injected at the same bus; $\bar{\chi}_{hk}$ is the CF of the admittance \bar{Y}_{hk} ; and $\bar{\chi}_{hh}$ is the CF of the admittance \bar{Y}_{hh} , equal to:

$$\bar{\chi}_{hh} = -\frac{\sum_{k \in \mathbb{B}_h} \bar{Y}_{hk} \bar{\chi}_{hk}}{\bar{Y}_{hh}}. \quad (7)$$

Solving (6) for $\bar{\eta}_h$ and rearranging some terms:

$$\bar{\eta}_h = \sum_{k \in \mathbb{B}_h} \frac{(\bar{v}_h - \bar{v}_k) \bar{Y}_{hk} \bar{\chi}_{hk}}{\bar{v}_h \bar{Y}_{hh}} - \sum_{k \in \mathbb{B}_h} \frac{\bar{v}_k \bar{Y}_{hk} \bar{\eta}_k}{\bar{v}_h \bar{Y}_{hh}} - \frac{\bar{i}_h \bar{\xi}_h}{\bar{v}_h \bar{Y}_{hh}}. \quad (8)$$

Recalling (3), (8) becomes:

$$\bar{\eta}_h = \sum_{k \in \mathbb{B}_h} \frac{\bar{i}_{h \rightarrow k} \bar{\chi}_{hk}}{\bar{v}_h \bar{Y}_{hh}} - \sum_{k \in \mathbb{B}_h} \frac{\bar{v}_k \bar{Y}_{hk} \bar{\eta}_k}{\bar{v}_h \bar{Y}_{hh}} - \frac{\bar{i}_h \bar{\xi}_h}{\bar{v}_h \bar{Y}_{hh}}. \quad (9)$$

Let us define the quantities $\bar{c}_{\chi_{hk}}$, $\bar{c}_{\eta_{hk}}$ and \bar{c}_{ξ_h} as:

$$\bar{c}_{\chi_{hk}} = \frac{\bar{v}_{h \rightarrow k}}{\bar{v}_h \bar{Y}_{hh}}, \quad \bar{c}_{\eta_{hk}} = -\frac{\bar{v}_k \bar{Y}_{hk}}{\bar{v}_h \bar{Y}_{hh}}, \quad \bar{c}_{\xi_h} = \frac{-\bar{i}_h}{\bar{v}_h \bar{Y}_{hh}}. \quad (10)$$

Then, (9) leads to the sought expression of the CF of the bus voltages:

$$\bar{\eta}_h = \sum_{k \in \mathbb{B}_h} \bar{c}_{\chi_{hk}} \bar{\chi}_{hk} + \sum_{k \in \mathbb{B}_h} \bar{c}_{\eta_{hk}} \bar{\eta}_k + \bar{c}_{\xi_h} \bar{\xi}_h \quad (11)$$

In (11), the CF of the voltage of a certain bus h is expressed as a linear combination of the CF of three different types of variables: admittance connected to h , weighted by a complex coefficient $\bar{c}_{\chi_{hk}}$, adjacent voltages, weighted by a complex coefficient $\bar{c}_{\eta_{hk}}$, and the net current injected at the node, weighted by the complex coefficient \bar{c}_{ξ_h} .

The coefficients of (11) can be interpreted as a measure of the participation of three elements to the dynamic of the voltage: series branches ($\bar{c}_{\chi_{hk}}$), neighboring bus voltages ($\bar{c}_{\eta_{hk}}$) and net current injections (\bar{c}_{ξ_h}). Valuable information can be extracted by analyzing the characteristics of these complex coefficients. For example, the real part of $\bar{c}_{\eta_{hk}}$ can be viewed as a measure of the self-participation of neighbor voltages on the CF of every bus. In other words, the real part of $\bar{c}_{\eta_{hk}}$ measures how much ρ_k affects ρ_h and ω_k affects ω_h . On the other hand, the imaginary part of $\bar{c}_{\eta_{hk}}$ represents the cross-participation, i.e., how much neighbor ρ_k affects ω_h and ω_k affects ρ_h . Hence, it is to be expected that the real part of $\bar{c}_{\eta_{hk}}$ is greater than its imaginary part, i.e., a small $\rho \leftrightarrow \omega$ dynamic coupling compared to the $\rho \leftrightarrow \rho$ and $\omega \leftrightarrow \omega$ direct link between two consecutive buses. Moreover, we note that all the coefficients in (11) are dimensionless since they relate normalized variations of different variables expressed in terms of CFs. While the concept of the CF of the current $\bar{\xi}$ and the voltage $\bar{\eta}$ has been comprehensively explained in [9], the value of $\bar{\chi}$ depends on what is actually being modeled as a time-varying admittance. For instance, dynamic series devices such as regulating transformers, AC/DC converters, or simply RLC dynamics. These examples are studied in the following section. To complete this section, we note that, for constant admittances, (11) reduces to:

$$\bar{\eta}_h = \sum_{k \in \mathbb{B}_h} \bar{c}_{\eta_{hk}} \bar{\eta}_k + \bar{c}_{\xi_h} \bar{\xi}_h. \quad (12)$$

Then, for buses without a shunt-connected device, namely, transit buses, (11) reduces to a linear combination of only neighbor buses dynamics:

$$\bar{\eta}_h = \sum_{k \in \mathbb{B}_h} \bar{c}_{\eta_{hk}} \bar{\eta}_k. \quad (13)$$

IV. MODELING OF TIME-VARYING BRANCHES

Specific expressions for $\bar{\chi}$ are derived in this section for different cases of dynamic admittances.

A. Dynamic RLC Branches

Consider the circuit shown in the left side of Fig. 1.

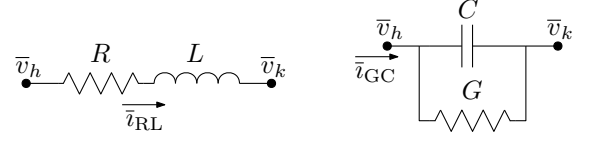


Fig. 1: Left: series RL circuit; right: parallel GC circuit.

The well-known equation that links the current and the voltage applied to a series RL circuit is:

$$L \dot{i}_{RL} + R i_{RL} = \bar{v}_h - \bar{v}_k. \quad (14)$$

Using the CF as a derivative operator:

$$L \bar{i}_{RL} \bar{\xi} + R \bar{i}_{RL} = \bar{v}_h - \bar{v}_k, \quad (15)$$

$$\bar{i}_{RL} (L \bar{\xi} + R) = \bar{v}_h - \bar{v}_k, \quad (16)$$

$$\bar{i}_{RL} = \frac{1}{L \bar{\xi} + R} (\bar{v}_h - \bar{v}_k), \quad (17)$$

$$\Rightarrow \bar{Y}_{RL} = \frac{1}{L \bar{\xi} + R}. \quad (18)$$

Thus, $\bar{\chi}_{RL}$ can be written as:

$$\bar{\chi}_{RL} = \frac{\dot{\bar{Y}}_{RL}}{\bar{Y}_{RL}} \Rightarrow \boxed{\bar{\chi}_{RL} = -\frac{\dot{\bar{\xi}}}{\bar{\xi} + \frac{R}{L}}} \quad (19)$$

Following a similar procedure, it can be shown that the admittance of a dynamic parallel GC branch, as shown in the right circuit of Fig. 1, is:

$$\bar{Y}_{GC} = C \bar{\eta} + G, \quad (20)$$

where $\bar{\eta}$ is the CF of the voltage applied between both terminals of the GC block, i.e., $(\bar{v}_h - \bar{v}_k)$. Finally, $\bar{\chi}_{GC}$ is obtained as:

$$\bar{\chi}_{GC} = \frac{\dot{\bar{Y}}_{GC}}{\bar{Y}_{GC}} \Rightarrow \boxed{\bar{\chi}_{GC} = \frac{\dot{\bar{\eta}}}{\bar{\eta} + \frac{G}{C}}} \quad (21)$$

For lossless circuits, (19) and (21) become:

$$\bar{\chi}_{RL}|_{R=0} = -\frac{\dot{\bar{\xi}}}{\bar{\xi}}, \quad \text{and} \quad \bar{\chi}_{GC}|_{G=0} = \frac{\dot{\bar{\eta}}}{\bar{\eta}}. \quad (22)$$

The CF of RLC series connections, PI-type lines, or any other dynamic circuit composed of a combination of these basic blocks can be derived using the equations provided in this subsection.

B. Regulating Transformer

Regulating transformers are series-connected devices that can modify the magnitude and-or the phase angle difference between two nodes of a meshed network. Regardless its control scheme, the regulating transformer can be modeled as a series of an ideal transformer with a variable complex tap ratio and an admittance [20]. A graphical representation of the circuit is shown in Fig. 2.

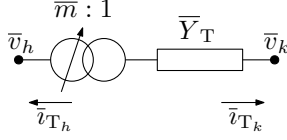


Fig. 2: Regulating transformer equivalent circuit.

In Fig. 2, $\bar{m} = me^{j\alpha}$ represents the complex tap ratio and \bar{Y}_T is the admittance of the transformer. The link between the terminal voltages and currents can be written in terms of a non-symmetric admittance matrix $\bar{\mathbf{Y}}_T$ as follows [20]:

$$\begin{bmatrix} \bar{i}_{T_k} \\ \bar{i}_{T_h} \end{bmatrix} = \begin{bmatrix} -\bar{Y}_T & me^{j\alpha}\bar{Y}_T \\ me^{-j\alpha}\bar{Y}_T & -m^2\bar{Y}_T \end{bmatrix} \begin{bmatrix} \bar{v}_k \\ \bar{v}_h \end{bmatrix} = \bar{\mathbf{Y}}_T \begin{bmatrix} \bar{v}_k \\ \bar{v}_h \end{bmatrix}. \quad (23)$$

Then, $\bar{\chi}$ is calculated for each term of the admittance matrix of the regulating transformer by imposing the following equation:

$$\dot{\bar{\mathbf{Y}}}_T = \bar{\mathbf{X}}_T \circ \bar{\mathbf{Y}}_T, \quad (24)$$

where the dot over the matrix denotes the time derivative of each matrix element, and \circ represents the Hadamard product, i.e., the element-by-element product of the two matrices; and $\bar{\mathbf{X}}_T$ is:

$$\bar{\mathbf{X}}_T = \begin{bmatrix} 0 & \frac{\dot{m}}{m} + j\dot{\alpha} \\ \frac{\dot{m}}{m} - j\dot{\alpha} & 2\frac{\dot{m}}{m} \end{bmatrix} \quad (25)$$

C. AC-DC Converter

Figure 3 shows a typical scheme of an AC/DC converter, which includes a bidirectional ideal converter and a transformer on the AC side of the converter.

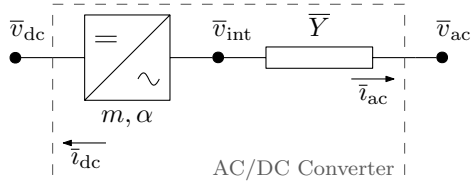


Fig. 3: AC/DC converter graphical representation.

Note that \bar{v}_{dc} and \bar{i}_{dc} are assumed to be complex quantities, although their phase angle is null, to allow for a general formulation of hybrid AC/DC systems. Neglecting the magnetization and the iron losses of the transformer, the electrical equations of the averaged model of the converter are [21]:

$$\bar{v}_{int} = \bar{v}_{dc}\bar{m}, \quad (26)$$

$$\bar{m} = me^{j(\theta_{ac} + \alpha)}, \quad (27)$$

$$\bar{i}_{ac} = (\bar{v}_{int} - \bar{v}_{ac})\bar{Y}, \quad (28)$$

$$0 = \Re\{\bar{v}_{dc}\bar{i}_{dc}\} + \Re\{\bar{v}_{int}\bar{i}_{ac}^*\}, \quad (29)$$

where, using the notation of Fig. 3, m is the scaling factor of the AC/DC converter; α is the phase shift the AC/DC converter introduces between AC node $\bar{v}_{ac} = v_{ac}\angle\theta_{ac}$ and the internal node \bar{v}_{int} ; and \bar{Y} is the series admittance of the filter and transformer on the AC side of the converter. Note that, while

the rectangular form is the most common representation of \bar{m} in the literature, i.e., $\bar{m} = m_d + jm_q$, we have nevertheless utilized the polar form shown in (27) for consistency with the formulation of the other models.

It is important to remark that the derivation that follows is valid independently from the control scheme implemented in the converter. This is due to the fact that the admittance block and, thus, $\bar{\chi}$, depend only on the electrical equations of the AC/DC converter (26)-(29). Thus, the dynamics of the controllers are implicitly reflected in \bar{m} .

Differentiating $\bar{\chi}$ requires prior knowledge of the equivalent admittance block of the converter. One approach to obtain this block is to first represent the AC/DC converter model as an equivalent circuit, which requires including additional elements to be consistent with (26)-(29). Examples of this strategy can be found in [22] and [23], where a shunt susceptance is included to balance the reactive power. An alternative, more direct approach, which we use in this work, is to manipulate (26)-(29) to obtain the following form:

$$\begin{bmatrix} \bar{i}_{ac} \\ \bar{i}_{dc} \end{bmatrix} = \begin{bmatrix} \bar{Y}_{acac} & \bar{Y}_{acdc} \\ \bar{Y}_{dcac} & \bar{Y}_{dc dc} \end{bmatrix} \begin{bmatrix} \bar{v}_{ac} \\ \bar{v}_{dc} \end{bmatrix}. \quad (30)$$

By taking the first row of (30):

$$\bar{i}_{ac} = \bar{Y}_{acac}\bar{v}_{ac} + \bar{Y}_{acdc}\bar{v}_{dc}. \quad (31)$$

On the other hand, from (28) and using (26):

$$\bar{i}_{ac} = -\bar{Y}\bar{v}_{ac} + \bar{m}\bar{Y}\bar{v}_{dc}. \quad (32)$$

Comparing (31) and (32), \bar{Y}_{acac} and \bar{Y}_{acdc} are found:

$$\bar{Y}_{acac} = -\bar{Y}, \quad (33)$$

$$\bar{Y}_{acdc} = me^{j(\alpha + \theta_{ac})}\bar{Y}. \quad (34)$$

Next, by taking the second row of (30) and splitting the real and imaginary part:

$$i_{dc} = \Re\{\bar{Y}_{dcac}\}\Re\{\bar{v}_{ac}\} - \Im\{\bar{Y}_{dcac}\}\Im\{\bar{v}_{ac}\} + \Re\{\bar{Y}_{dc dc}\}v_{dc}, \quad (35)$$

$$0 = \Re\{\bar{Y}_{dcac}\}\Im\{\bar{v}_{ac}\} + \Im\{\bar{Y}_{dcac}\}\Re\{\bar{v}_{ac}\} + \Im\{\bar{Y}_{dc dc}\}v_{dc}. \quad (36)$$

On the other hand, from (29) and using (26) and (28):

$$0 = v_{dc}i_{dc} + v_{dc}\Re\{\bar{m}\bar{i}_{ac}^*\}, \quad (37)$$

$$i_{dc} = -\Re\left\{\bar{m}(\bar{v}_{int}^* - \bar{v}_{ac}^*)\bar{Y}^*\right\}, \quad (38)$$

$$i_{dc} = -\Re\left\{\bar{m}^*(\bar{m}v_{dc} - \bar{v}_{ac})\bar{Y}\right\}, \quad (39)$$

$$i_{dc} = \Re\left\{-m^2\bar{Y}\right\}v_{dc} + \Re\left\{\bar{Y}\bar{m}^*\bar{v}_{ac}\right\}, \quad (40)$$

$$i_{dc} = \Re\left\{\bar{Y}\bar{m}^*\right\}\Re\{\bar{v}_{ac}\} - \Im\left\{\bar{Y}\bar{m}^*\right\}\Im\{\bar{v}_{ac}\} + \dots \quad (41)$$

$$\dots + \Re\left\{-m^2\bar{Y}\right\}v_{dc}.$$

Considering $\bar{Y} = Ye^{j\gamma} = G + jB$, and comparing (35) and (41):

$$\bar{Y}_{dcac} = \bar{Y}\bar{m}^* = me^{-j(\alpha + \theta_{ac})}\bar{Y}, \quad (42)$$

$$\Re\{\bar{Y}_{dc dc}\} = \Re\left\{-m^2\bar{Y}\right\} = -m^2G. \quad (43)$$

Replacing (42) in (36):

$$0 = \Im\{\bar{Y}\bar{m}^*\bar{v}_{ac}\} + \Im\{\bar{Y}_{dcdc}\}v_{dc}, \quad (44)$$

$$\Im\{\bar{Y}_{dcdc}\} = -\Im\left\{\frac{\bar{Y}\bar{m}^*\bar{v}_{ac}}{v_{dc}}\right\}, \quad (45)$$

$$\Im\{\bar{Y}_{dcdc}\} = jm\frac{v_{ac}}{v_{dc}}Y\sin(\alpha - \gamma), \quad (46)$$

$$\Im\{\bar{Y}_{dcdc}\} = jm\frac{v_{ac}}{v_{dc}}(G\sin(\alpha) - B\cos(\alpha)). \quad (47)$$

Finally, the equivalent admittance block of the AC/DC converter is obtained as follows:

$$\bar{Y}_{acdc} = \begin{bmatrix} \bar{Y}_{acac} & \bar{Y}_{acdc} \\ \bar{Y}_{dcac} & \bar{Y}_{dcdc} \end{bmatrix}, \quad (48)$$

where:

$$\bar{Y}_{acac} = -\bar{Y}, \quad (49)$$

$$\bar{Y}_{acdc} = me^{j(\alpha+\theta_{ac})}\bar{Y}, \quad (50)$$

$$\bar{Y}_{dcac} = me^{-j(\alpha+\theta_{ac})}\bar{Y}, \quad (51)$$

$$\bar{Y}_{dcdc} = -m^2G + jm\frac{v_{ac}}{v_{dc}}(G\sin(\alpha) - B\cos(\alpha)). \quad (52)$$

Then, $\bar{\chi}$ is calculated for each term of \bar{Y}_{acdc} by imposing:

$$\dot{\bar{Y}}_{acdc} = \bar{X}_{acdc} \circ \bar{Y}_{acdc}. \quad (53)$$

The calculation of $\bar{\chi}_{acac}$, $\bar{\chi}_{acdc}$, $\bar{\chi}_{dcac}$ is analogous to the calculations of the coefficients of the regulating transformer:

$$\bar{\chi}_{acac} = 0 \quad (54)$$

$$\bar{\chi}_{acdc} = \frac{\dot{m}}{m} + j(\dot{\alpha} + \dot{\theta}_{ac}) \quad (55)$$

$$\bar{\chi}_{dcac} = \frac{\dot{m}}{m} - j(\dot{\alpha} + \dot{\theta}_{ac}) \quad (56)$$

On the other hand, the term $\bar{\chi}_{dcdc}$ requires more work. First, \bar{Y}_{dcdc} is separated as the following:

$$\bar{Y}_{dcdc} = \bar{Y}_{dcdc}^{(1)} + \bar{Y}_{dcdc}^{(2)}, \quad (57)$$

$$\bar{Y}_{dcdc}^{(1)} = -m^2G, \quad (58)$$

$$\bar{Y}_{dcdc}^{(2)} = jm\frac{v_{ac}}{v_{dc}}(G\sin(\alpha) - B\cos(\alpha)), \quad (59)$$

$$\Rightarrow \bar{\chi}_{dcdc} = \frac{\bar{Y}_{dcdc}^{(1)}\bar{\chi}_{dcdc}^{(1)} + \bar{Y}_{dcdc}^{(2)}\bar{\chi}_{dcdc}^{(2)}}{\bar{Y}_{dcdc}^{(1)} + \bar{Y}_{dcdc}^{(2)}}, \quad (60)$$

where

$$\bar{\chi}_{dcdc}^{(1)} = 2\frac{\dot{m}}{m}, \quad (61)$$

$$\bar{\chi}_{dcdc}^{(2)} = \frac{\dot{m}}{m} + \frac{\dot{v}_{ac}}{v_{ac}} - \frac{\dot{v}_{dc}}{v_{dc}} + \dot{\alpha}\frac{G\cos(\alpha) + B\sin(\alpha)}{G\sin(\alpha) - B\cos(\alpha)}. \quad (62)$$

If losses are neglected, $\bar{\chi}_{dcdc}$ becomes:

$$\bar{\chi}_{dcdc}|_{G=0} = \frac{\dot{m}}{m} + \frac{\dot{v}_{ac}}{v_{ac}} - \frac{\dot{v}_{dc}}{v_{dc}} - \dot{\alpha}\tan(\alpha) \quad (63)$$

V. CASE STUDIES

In this section, we apply the proposed general expression (11) for the CF as well as the various model-dependent expressions derived in Section IV to three benchmark systems. In Section V-A, we use a purely AC system to present a steady-state analysis of the values of the coefficients of (11). In Section V-B, we use a DC network to present a dynamic analysis focused on the coefficients of our equation regarding dynamic RLC branches. In Section V-C, we present a hybrid system including different types of time-varying branches described in Section IV, namely RLC dynamic branches and AC/DC converters. We also show the ability of our general formulation to study together such a diverse system and the different ways the AC/DC converter propagates the frequency dynamics depending on its control mode. Finally, Section V-D collects remarks on practical applications of the proposed modeling approach.

A. AC System

The proposed formulation is applied to the WSCC 9-bus benchmark system. The network consists of three synchronous generators feeding three loads through a delta-type topology. The single-line diagram of the WSCC system is shown in Fig. 4.

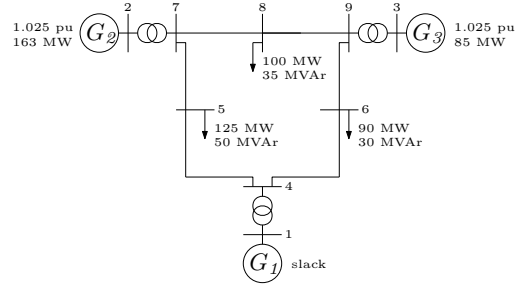


Fig. 4: Single-line diagram of the WSCC 9-bus system.

Let us consider first the case of an admittance matrix with constant elements. Thus, we use the simplified expression (12). The power flow solution is found for the base-case operating conditions shown in Fig. 4. The solution is used to calculate $\bar{c}_{\eta_{hk}}$ and \bar{c}_{ξ_h} for every bus h . The steady-state coefficients given by the power flow solution are shown in Table I.

Columns 2-10 of the table show the participation of neighbor buses to the CF of every bus. Elements corresponding to non-neighbor buses are null, as expected, and left blank in the table. The table is sparse in the same way the admittance matrix of a system is sparse, i.e., rather than an absolute measure of the relationship between every pair of buses, the information has the same structure of the connectivity matrix of the grid. Thus, even if a coefficient linking a given pair of buses is null, the voltage variations in one bus impact on the voltage of the other bus though the intermediate bus connections. The coefficients $\bar{c}_{\eta_{hk}}$ are predominantly real, which means that, as expected, the results verify a small $\rho \leftrightarrow \omega$ dynamic coupling compared to the $\rho \leftrightarrow \rho$ and $\omega \leftrightarrow \omega$ direct link. The impact of the net injected current is shown in the last column of Table I. As this coefficient is proportional to

TABLE I: Steady state coefficients of the CF for the WSCC 9-bus system.

Bus	$\bar{c}_{\eta_{h1}}$	$\bar{c}_{\eta_{h2}}$	$\bar{c}_{\eta_{h3}}$	$\bar{c}_{\eta_{h4}}$	$\bar{c}_{\eta_{h5}}$	$\bar{c}_{\eta_{h6}}$	$\bar{c}_{\eta_{h7}}$	$\bar{c}_{\eta_{h8}}$	$\bar{c}_{\eta_{h9}}$	\bar{c}_{ξ_h}
1	-	-	-	0.99-j0.04	-	-	-	-	-	0.01+j0.04
2	-	-	-	-	-	-	1.00-j0.10	-	-	0.00+j0.10
3	-	-	-	-	-	-	-	-	1.01-j0.05	-0.01+j0.05
4	0.45-j0.02	-	-	-	0.29+j0.00	0.27+j0.02	-	-	-	-
5	-	-	-	0.69+j0.00	-	-	0.35+j0.07	-	-	-0.04-j0.07
6	-	-	-	0.67+j0.01	-	-	-	-	0.36+j0.04	-0.03-j0.05
7	-	0.45+j0.01	-	-	0.17+j0.00	-	-	0.38-j0.01	-	-
8	-	-	-	-	-	-	0.59+j0.03	-	0.43+j0.01	-0.02-j0.04
9	-	-	0.53-j0.02	-	-	0.17+j0.01	-	0.30+j0.01	-	-

the net current injected at the bus, buses with a shunt device interchanging more power exhibit a higher magnitude than those with less power. For instance, the magnitude of \bar{c}_{ξ_h} for bus 2, which has G_2 injecting 163 MW, is approximately twice compared to the value for bus 3, which has G_3 injecting 85 MW. In the case of transit buses 4, 7 and 9, \bar{c}_{ξ_h} is null. However, the coefficients \bar{c}_{ξ_h} are generally much smaller than the coefficients \bar{c}_{η_h} because of the different scaling between voltage and current coefficients. Thus, the different magnitudes are not an indication that the current injected by devices has a negligible impact on the voltage.

Property 1: It is interesting to note that a remarkable property of the coefficients is verified: for each bus, each row in Table I always sums exactly 1. The proof can be derived by taking (4) and dividing both sides by the left-hand side of the equation. This property has a physical interpretation: for every bus, the sum of the self-participation of neighbor buses and the net current injected naturally adds up to 100%, whereas the sum of the cross-participations vanishes.

Finally, as a sensibility analysis, the line connecting buses 7 and 8 is replaced by a regulating transformer to examine its corresponding coefficient according to (11). The model used is as described in IV-B, with a series resistance and inductance equal to the parameters of the original line. The tap ratio is set to 1, and the active power reference is set equal to the solution of the power flow of the original case. Under these conditions, the coefficients presented in Table I are unaltered. However, the coefficients modeling the dynamic effect of the regulating transformer also become relevant for buses 7 and 8. The resulting expression for the CF of bus 7 is:

$$\bar{\eta}_7 = \underbrace{\sum_{k \in \{2,5,8\}} \bar{c}_{\eta_{7k}} \bar{\eta}_k}_{\text{Original terms}} + \underbrace{\bar{c}_{\chi_{78}} \left(\frac{\dot{m}}{m} + j\dot{\alpha} \right)}_{\text{Regulating transformer term}} \quad (64)$$

where $\bar{c}_{\chi_{78}} = -(0.01 + 0.03j)$. Note that $\bar{c}_{\chi_{78}}$, which weights the impact of the control of the regulating transformer on $\bar{\eta}_7$ has a small magnitude, and has same order of magnitude of the coefficients \bar{c}_{ξ} of the net injected current. However, since the control of the regulating transformer is “slow”, one has to expect that its effect on $\bar{\eta}_7$ is small.

B. DC System

The proposed expression (11) is utilized for the DC subsystem of the hybrid Chaudhuri’s Multi-terminal DC (MTDC) system [24]. This subsystem consists of a 4-bus 350 kV DC grid with four converter stations, each connected to an equivalent AC grid. The scheme of the DC subsystem is shown in Fig. 5. The original data are modified by including an auxiliary RL branch between nodes N2 and N3 with ten times the resistance and inductance of the existing connection. The perturbation consists in disconnecting the auxiliary RL branch.

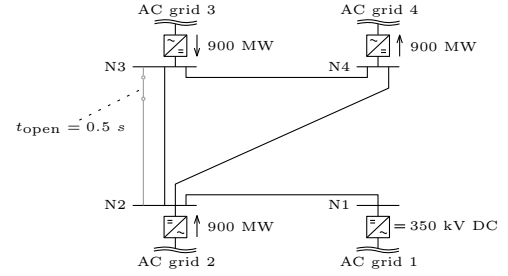


Fig. 5: Scheme of the DC subsystem of the Chaudhuri’s MTDC system.

The DC transmission system is modeled considering series resistance, inductance, and shunt capacitance of all branches. A time-domain simulation is carried out to study how the coefficients of (11), especially those capturing line dynamic effects, vary during the transient.

Starting from the operating point given by the conditions shown in Fig. 5, the auxiliary RL branch is disconnected at $t = 0.5$ s. The trajectories of the voltages of the four DC nodes is shown in Fig. 6. The perturbation causes an oscillation of about 27 Hz which is due to the coupling of branch inductances and capacitances. These oscillations are noticeable on the DC voltage of every bus except N1. This happens because the d -axis control loop configured in converter one actively controls the DC voltage with a faster time constant than the dynamics triggered by the perturbation.

The trajectories of the real part of the coefficients of (11) for N3 is shown in Figs. 7 and 8. The imaginary part is null for the DC grid. As expected, since all the coefficients depend on the system variables, they inherit the dynamic triggered by the perturbation. Figure 8 indicates that the

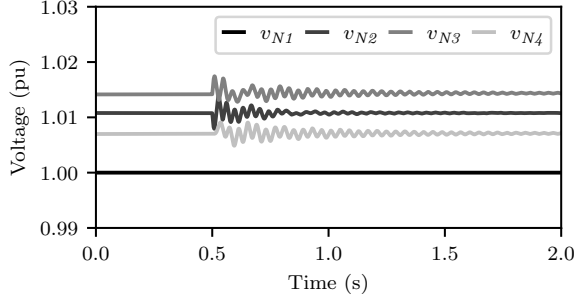


Fig. 6: Trajectories of the voltages of DC nodes.

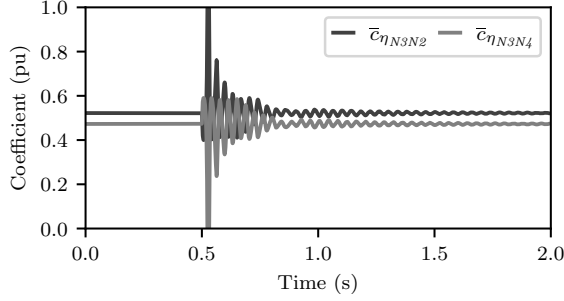


Fig. 7: Trajectories of the real part of the coefficients corresponding to the neighbor voltages for N3.

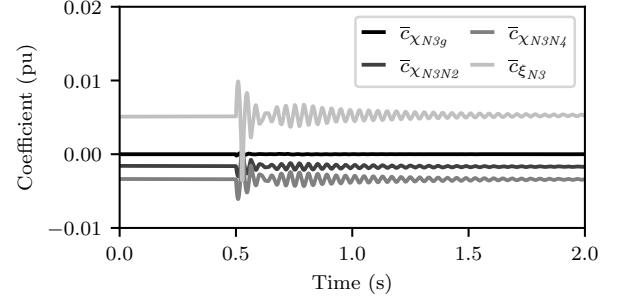


Fig. 8: Trajectories of the real part of the coefficients corresponding to dynamic branches and net current injected coefficients for N3.

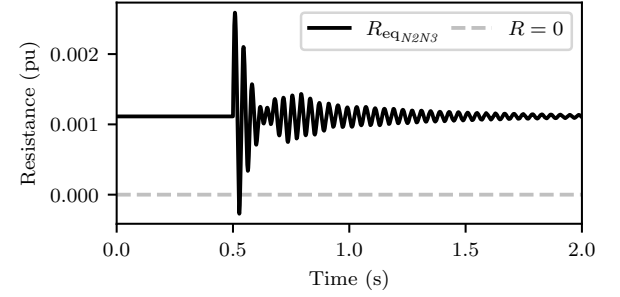


Fig. 9: Trajectories of the equivalent resistance of branch N2-N3.

coefficient related to the dynamic of shunt capacitance blocks ($\bar{c}_{\chi_{N3g}}$) is considerably lower and almost negligible than those corresponding to series inductance blocks. This difference is due to the current flowing through each branch.

Property 2: It is also interesting to observe another property of the proposed expression (11): the sum of all the coefficients corresponding to the time-varying branches ($\bar{c}_{\chi_{N3N2}} + \bar{c}_{\chi_{N3N4}}$) equals the value of the net injected current coefficient ($\bar{c}_{\xi_{N3}}$). This property can also be obtained from (3) and the definition of the coefficients $\bar{c}_{\chi_{hk}}$ given in (10).

Finally, note that $\bar{c}_{\eta_{N3N2}}$, $\bar{c}_{\eta_{N3N4}}$ and $\bar{c}_{\xi_{N3}}$ exhibit a spike in the second oscillation peak after the perturbation. The rationale behind this phenomenon lies in the fact that the modeling approach presented in Section IV uses instantaneous equivalent admittance blocks that depend on variable CF quantities. In particular, (18) shows that for an RL branch, the equivalent admittance equals the inverse of $(L\bar{\xi} + R)$. Consequently, it is possible to have a singularity in case $(L\bar{\xi} + R) = 0$. In the case of AC grids, the issue does not occur due to the imaginary part of $\bar{\xi}$, which corresponds to the instantaneous frequency of the current. However, in DC grids, $(L\bar{\xi} + R)$ is real and can be viewed as an equivalent resistance with expression:

$$R_{eq} = L \frac{i}{l} + R. \quad (65)$$

To illustrate this peculiar behavior, Fig. 9 shows the equivalent resistance R_{eq} of branch N2-N3, which change sign in correspondence of the spike of the trajectories shown in Fig. 7.

C. Hybrid AC/DC System

Here we illustrate the behavior of the elements of the proposed formula (11) for the complete hybrid Chaudhuri's MTDC system [24]. A multi-terminal DC (MTDC) system is connected to the grid through two different buses. The DC grid is also connected to two remote isolated AC grids. The main AC grid consists of a multi-machine AC network with two areas, two synchronous generators each. The MTDC system injects real power into the main AC grid. The system's single-line diagram is shown in Fig. 10.

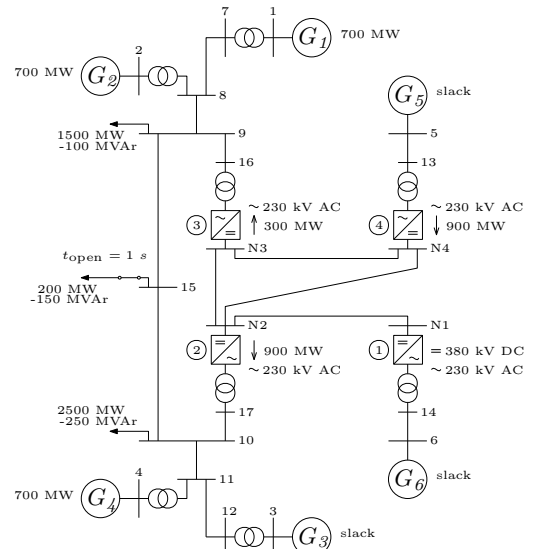


Fig. 10: Single-line diagram of the Chaudhuri's MTDC system.

The DC lines are modeled considering series resistance, inductance, and shunt capacitance, as described in Section V-B. For simplicity but without lack of generality, the AC transmission system is modeled as a constant admittance matrix. Besides, the four AC/DC converters are modeled as in Section IV-C plus different control schemes. Their controlled variables are shown in Table II for each device. While converters 2 and 3 contribute to the frequency regulation in the main AC area, converter 4 supports the frequency of the isolated AC grid it is connected to. Converter 1 sustains the DC voltage instead of having a frequency-control loop. Finally, all the synchronous generators are equipped with standard governors and AVR models. There is also an AGC in the three AC areas.

TABLE II: Control modes configured in each converter.

Control Loop	Converter			
	1	2	3	4
d -axis (P-control)	v_{dc}	f_{ac}	f_{ac}	f_{ac}
q -axis (Q-control)	v_{ac}	v_{ac}	v_{ac}	v_{ac}

A time-domain simulation is carried out to study the relationship between the CF of AC and DC buses based on the proposed equation. In particular, we show the effect of the AC/DC converter model depending on the control mode configured on each converter. The contingency is a sudden disconnection of the load connected at bus 15 at $t = 1$ s. Figures 11 and 12 show the evolution of the frequency of the COI of the three AC areas and the DC RoCoV at the four DC nodes, respectively. As expected, the frequency of the main AC area (f_{COI_1}) increases after the load disconnection. Consequently, converters 2 and 3 reduce their power injection, leading to a deviation in the DC voltage at N2 and N3. The AC dynamic propagates through the DC network to converters 1 and 4, which show different behaviors. Converter 4 observes a dynamic event at N4, but it does not propagate it to the AC side, i.e., f_{COI_2} is constant. On the other hand, converter 1 keeps a constant DC voltage at N1 ($\rho_{N1} = 0$), but current variations propagate the dynamic event to the AC side, leading to a significant frequency deviation in that area (f_{COI_3}). The difference lies in the dynamics of m and α according to the control mode of each converter.

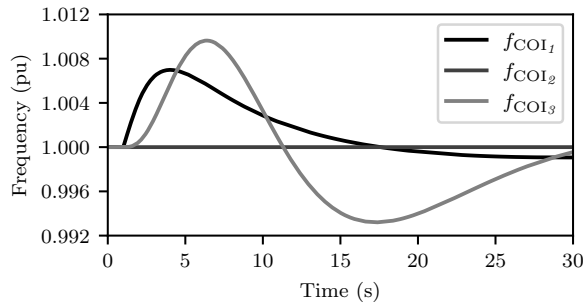


Fig. 11: Trajectories of the COI-frequencies of the three AC areas of the Chaudhuri's MTDC system.

Equation (11) is implemented at buses 13 and 14 to explain the effect of the control of converters 1 and 4. Since our for-

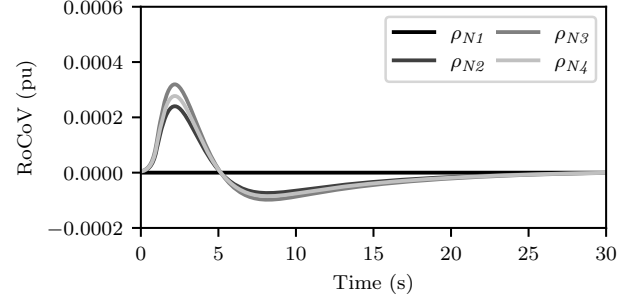


Fig. 12: Trajectories of the DC RoCoVs of the Chaudhuri's MTDC system.

mulation allows us to treat the AC/DC converters as branches, buses 13 and 14 become transit buses, and thus, (11) becomes:

$$\bar{\eta}_h = \sum_{k \in \mathbb{B}_h} \bar{c}_{\chi_{hk}} \bar{\chi}_{hk} + \sum_{k \in \mathbb{B}_h} \bar{c}_{\eta_{hk}} \bar{\eta}_k \quad (66)$$

In the case of bus 13, the only non-null terms of (66) are those corresponding to adjacent buses: $\bar{\eta}_{05}$, $\bar{\eta}_{N4}$, and the AC-DC converter: $\bar{\chi}_{13N4}$. The time evolution of the real and imaginary parts of these three CFs is shown in Fig. 13. The dynamic caused by the contingency is seen by converter 4 at the DC bus in the real part of $\bar{\eta}_{N4}$. The imaginary part is zero by definition (DC bus). The reaction of the converter is expressed through $\bar{\chi}_{13N4}$. Despite the different magnitudes, the real part of $\bar{\chi}_{13N4}$ exhibits the same dynamic but with an opposed sign.

The adjacent AC bus remains unaltered, i.e., it shows a zero real part and a constant unit imaginary part. The contribution of the three CFs is multiplied by the corresponding complex coefficients and added according to (66) to give $\bar{\eta}_{13}$. The time evolution of $\bar{\eta}_{13}$ is shown in Fig. 15. The effect of the converter is such that it compensates the dynamic received at N4, thus giving an unaltered $\bar{\eta}$ at bus 13, i.e., zero real part and unit imaginary part. In other words, the DC dynamic does not propagate to the AC side.

In the case of bus 14, the only non-null terms of (66) are those corresponding to adjacent buses: $\bar{\eta}_{06}$, $\bar{\eta}_{N1}$, and the AC-DC converter: $\bar{\chi}_{14N1}$. The trajectories of the real and imaginary parts of these three CFs are shown in Fig. 14. In this case, the real part of the CF at the DC bus $\bar{\eta}_{N1}$ is nearly zero as converter 1 controls the DC voltage. However, this requires the converter to move its control variables, thus inducing a dynamic in both the real and imaginary parts of $\bar{\chi}_{13N1}$, which is finally propagated to the AC side. Fig. 15 shows the result for $\bar{\eta}_{14}$. In this case, the converter does propagate the dynamic to the AC side.

D. Remarks and Applications

The steady-state analysis of the coefficients of the proposed expression (11) given in Section V-A illustrates how these coefficients are useful dimensionless weights of the participation of adjacent buses to the dynamic of the voltage of a particular bus. Moreover, the ratio between the real and imaginary parts indicates the instantaneous coupling between ρ and ω . On

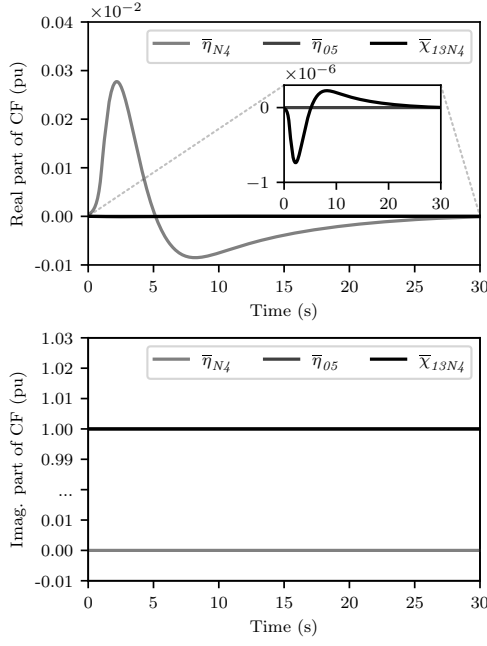


Fig. 13: Trajectories of the CFs of non-null terms of (66) for bus 13 of the Chaudhuri's MTDC system.

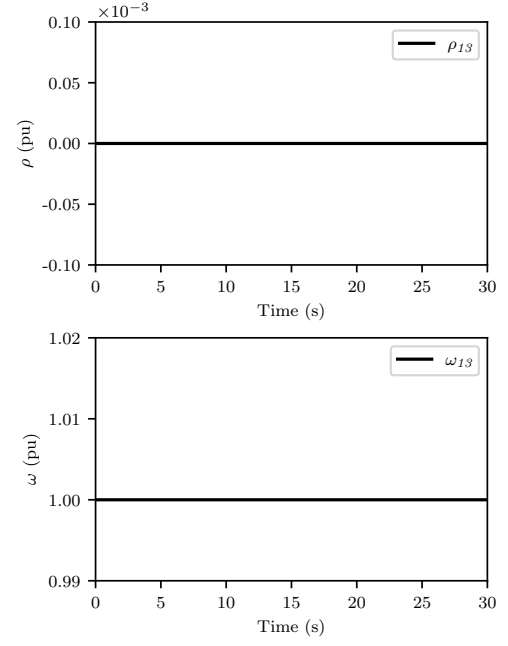


Fig. 15: Trajectories of the CF at bus 13 of the Chaudhuri's MTDC system. Calculated using equation (11).

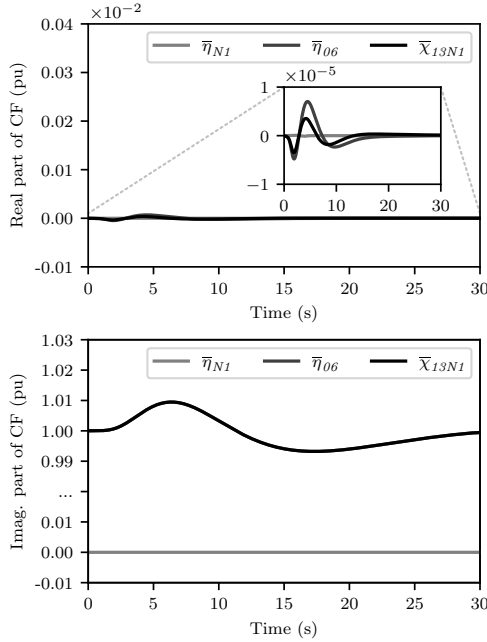


Fig. 14: Trajectories of the CFs of non-null terms of (66) for bus 14 of the Chaudhuri's MTDC system.

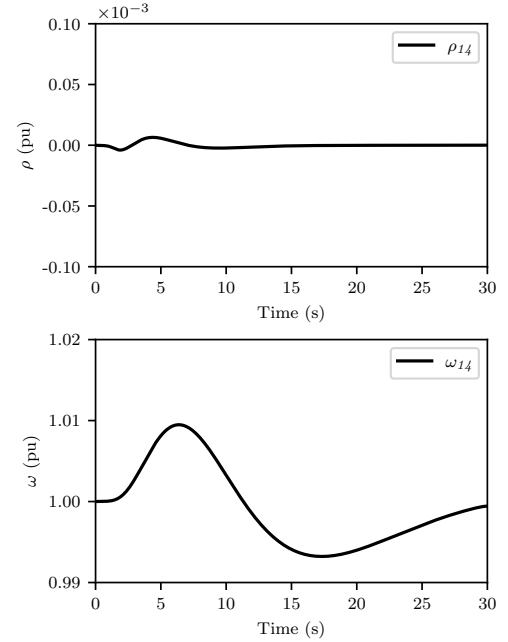


Fig. 16: Trajectories of the CF at bus 14 of the Chaudhuri's MTDC system. Calculated using equation (11).

the one hand, estimating the value of the coefficients appears useful for monitoring the power system state, especially for weak interconnections. On the other hand, taking their value as an input for a control scheme arises as an application worth exploring. Dynamic analysis shows that despite being affected by the dynamics of the system, the steady-state value of the coefficients of the expression tends to prevail. This confirms the potential use of the coefficients that appear in (11) as a metric to evaluate the level of synchronization between

adjacent buses.

The formulation of series elements of the network as dynamic admittances requires the definition of special quantities, which are useful for measuring some phenomena present in the system. For instance, the instantaneous equivalent resistance carries the information of the instantaneous energy exchange between L and R in an RL branch. The CFs of the dynamic admittances also appear as useful quantities to evaluate the dynamic impact of time-varying (e.g., controlled) series devices.

The proposed equation offers a quantitative framework for the analysis of time-domain simulation results. Particularly interesting is to explore its ability to evaluate the interaction between dynamic devices and the propagation of dynamics events. Notably, due to the exact nature of the formulation, this capability is model-agnostic, e.g. simulation of EMT or RMS models.

The dynamic admittance model used to represent AC/DC converters allows unifying the formulation of hybrid systems. Besides, the proposed equation explicitly relates the dynamics of the AC and DC side together with the effect of the converter. This opens the possibility of studying how to design a control scheme that achieves a specific objective of the propagation of ρ and ω . For instance, designing a control that translates the dynamic of ω of the AC side to ρ of the DC side and blocks the dynamic of ρ of the AC side at the same time. Such a scheme naturally transfer the information of the state of the frequency of a remote AC area throughout the DC grid without the need for communications.

VI. CONCLUSION

The paper introduces an explicit equation for the CF of the voltage in terms of the CF of three variables: the net current injected at the bus, the voltage of adjacent buses, and dynamic branches connected to the bus. The paper also provides specific expressions for dynamic RLC circuits, regulating transformers, and AC/DC converters. The representation of the AC/DC converter allows modeling hybrid systems in a unique formulation, and keeps track of the relationship between the dynamic behavior of the real and imaginary parts of the complex frequencies of the AC side and the DC side.

The case studies show that the proposed formulation is a useful tool to monitor the power system state, as the coefficients of (11) constitute a dimensionless measure of the dynamic link between adjacent buses. The novel quantities required to build the unique formulation presented in this paper can also be applied to quantify transient phenomena, such as the instantaneous energy exchange in a dynamic RL circuit or the reaction of active series branches. The latter case is especially promising in the case of AC/DC converters, where the formulation opens the possibility of designing a control scheme to achieve a specific objective of $\rho \leftrightarrow \omega$ propagation from AC to DC and vice-versa.

Future work will focus on the extension of the expression (11) to relevant devices, e.g., detailed models of grid-following and grid-following converters. Finally, upcoming research will explore applications of (11) for the monitoring, control and stability analysis of power systems.

REFERENCES

- [1] N. Hatziaargyriou *et al.*, "Definition and classification of power system stability – revisited & extended," *IEEE Transactions on Power Systems*, vol. 36, no. 4, pp. 3271–3281, 2021.
- [2] F. Milano, F. Dörfler, G. Hug, D. J. Hill, and G. Verbič, "Foundations and challenges of low-inertia systems (invited paper)," in *Power Systems Computation Conference (PSCC)*, pp. 1–25, 2018.
- [3] J. Fang, Y. Tang, H. Li, and F. Blaabjerg, "The role of power electronics in future low inertia power systems," in *IEEE International Power Electronics and Application Conference and Exposition (PEAC)*, pp. 1–6, 2018.

- [4] M. N. H. Shazon, Nahid-Al-Masood, and A. Jawad, "Frequency control challenges and potential countermeasures in future low-inertia power systems: A review," *Energy Reports*, vol. 8, pp. 6191–6219, 2022.
- [5] F. Dörfler and D. Groß, "Control of low-inertia power systems," *Annual Review of Control, Robotics, and Autonomous Systems*, vol. 6, pp. 415–445, 2023.
- [6] H. Kirkham, W. Dickerson, and A. Phadke, "Defining power system frequency," in *IEEE PES General Meeting (PESGM)*, pp. 1–5, 2018.
- [7] G. Frigo, A. Derviškić, and M. Paolone, "Impact of fundamental frequency definition in ipdft-based pmu estimates in fault conditions," in *IEEE 10th International Workshop on Applied Measurements for Power Systems (AMPS)*, pp. 1–6, 2019.
- [8] F. Milano and A. Ortega, *Frequency Variations in Power Systems: Modeling, State Estimation, and Control*. IEEE Press, Wiley, 2020.
- [9] F. Milano, "Complex frequency," *IEEE Transactions on Power Systems*, vol. 37, no. 2, pp. 1230–1240, 2022.
- [10] A. Büttner and F. Hellmann, "Complex couplings – a universal, adaptive and bilinear formulation of power grid dynamics," 2023.
- [11] F. Milano, B. Alhanjari, and G. Tzounas, "Enhancing frequency control through rate of change of voltage feedback," *IEEE Transactions on Power Systems*, pp. 1–4, 2023.
- [12] D. Moutevelis, J. Roldán-Pérez, M. Prodanovic, and F. Milano, "Design of virtual impedance control loop using the complex frequency approach," in *2023 IEEE Belgrade PowerTech*, pp. 1–6, IEEE, 2023.
- [13] X. He, V. Häberle, and F. Dörfler, "Complex-frequency synchronization of converter-based power systems," *arXiv preprint arXiv:2208.13860*, 2022.
- [14] X. He, V. Häberle, I. Subotić, and F. Dörfler, "Nonlinear stability of complex droop control in converter-based power systems," *IEEE Control Systems Letters*, vol. 7, pp. 1327–1332, 2023.
- [15] W. Zhong, G. Tzounas, and F. Milano, "Real-time estimation of vpp equivalent inertia and fast frequency control," in *IEEE PES General Meeting (PESGM)*, pp. 1–5, 2022.
- [16] W. Zhong, G. Tzounas, M. Liu, and F. Milano, "On-line inertia estimation of virtual power plants," *Electric Power Systems Research*, vol. 212, p. 108336, 2022.
- [17] D. Moutevelis, J. Roldán-Pérez, M. Prodanovic, and F. Milano, "Taxonomy of power converter control schemes based on the complex frequency concept," *IEEE Transactions on Power Systems*, pp. 1–13, 2023.
- [18] R. Mourouvin, K. Shinoda, J. Dai, A. Benchaib, S. Bacha, and D. Georges, "AC/DC dynamic interactions of MMC-HVDC in grid-forming for wind-farm integration in AC systems," in *22nd European Conference on Power Electronics and Applications (EPE'20 ECCE Europe)*, pp. 1–9, 2020.
- [19] F. Milano, "A geometrical interpretation of frequency," *IEEE Transactions on Power Systems*, vol. 37, no. 1, pp. 816–819, 2022.
- [20] P. Kundur, N. Balu, and M. Lauby, *Power System Stability and Control*. EPRI power system engineering series, McGraw-Hill Education, 1994.
- [21] F. Milano and A. Ortega, *Converter-Interfaced Energy Storage Systems: Context, Modelling and Dynamic Analysis*. Cambridge University Press, 2019.
- [22] M. M. Rezvani and S. Mehraeen, "A generalized model for unified ac-dc load flow analysis," in *2021 IEEE Texas Power and Energy Conference (TPEC)*, pp. 1–6, 2021.
- [23] E. Acha, B. Kazemtabrizi, and L. M. Castro, "A new vsc-hvdc model for power flows using the newton-raphson method," *IEEE Transactions on Power Systems*, vol. 28, no. 3, pp. 2602–2612, 2013.
- [24] N. Chaudhuri, B. Chaudhuri, R. Majumder, and A. Yazdani, *Multi-terminal Direct-Current Grids: Modeling, Analysis, and Control*. IEEE Press, Wiley, 2014.



Ignacio Ponce received from University of Chile the BSc. and MSc. degree in Electrical Engineering in 2019 and 2022, respectively. He is currently pursuing a Ph.D in Electrical Engineering at University College Dublin, Ireland. His research interests include power system modeling, control and stability analysis.



Federico Milano (F'16) received from the Univ. of Genoa, Italy, the Ph.D. in Electrical Engineering 2003. In 2013, he joined the University College Dublin, Ireland, where he is currently a full professor. He is Chair of the IEEE Power System Stability Controls Subcommittee, IET Fellow, IEEE PES Distinguished Lecturer, Chair of the Technical Program Committee of the PSCC 2024, Senior Editor of the IEEE Transactions on Power Systems, Member of the Cigré Irish National Committee, and Co-Editor in Chief of the IET Generation, Transmission &

Distribution. His research interests include power system modeling, control and stability analysis.